CONFORMATIONAL STRUCTURE OF AN ADSORBED POLYELECTROLYTE ON A NANOPARTICLE WITH LOW CONDUCTIVITY IN AN ALTERNATING ELECTRIC FIELD

Kucherenko M.G., Kruchinin N.Yu.*

Center of Laser and Informational Biophysics, Orenburg State University, Orenburg, Russian Federation,
kruchinin_56@mail.ru

An analytical form of the model of the quasi-equilibrium conformational structure of the units of the Gaussian chain of a polyelectrolyte adsorbed on a nanospheroid with a relatively low electrical conductivity (undoped semiconductor) polarized in an external harmonically varying quasi-static electric field with a frequency significantly lower than the plasma frequency of the nanoparticle material is proposed. Variants of the model are discussed that go beyond the scope of the quasi-static approximation, i.e., take into account the effects of delay, the manifestation of which will be noticeable in the case of sufficiently extended nanostructures. Electrically induced conformational changes of generally neutral polyampholytic polypeptides on the surface of a spherical germanium nanoparticle in a static or alternating external electric field have been studied by molecular dynamics. In a static electric field, in the case of a small distance between the charged units in the polyampholyte, a large number of macrochain loops were formed, elongated in the direction of the polarization axis of the nanoparticle. If the distance between the oppositely charged amino acid residues of the polypeptide exceeded the diameter of the nanoparticle, the charged units were mainly localized in the oppositely charged subpolar regions of the polarized germanium nanoparticle. In an alternating electric field, a girdle polyampholyte edge was formed in the equatorial region of the nanoparticle, the macrochain links of which were desorbed from the surface with an increase in the amplitude of the polarizing alternating electric field.

Keywords: semiconductor nanoparticle, macromolecule, conjugates, conformations, molecular dynamics.

1. Introduction

Conjugates of quantum dots with macromolecular chains are widely used as biological nanoprobes, as well as in the elements of various chemical sensors based on the use of the Förster energy transfer between nanoobjects connected by a macrochain [1–9]. In this aspect, of great interest is the control of the characteristics of such functional nanosystems by the action of an external electric field [10–13]. To this end, both generally neutral polyampholytic macromolecules and charged polyelectrolyte macrochains can be located on the surface of a nanoobject, the conformational structure of which can change under the influence of electric charges distributed over the surface of the nanoparticle.

Previously, in [14–21], conformational changes in polyampholytic polypeptides adsorbed on the surface of gold nanoparticles of various shapes (spherical, cylindrical, and spheroidal) were studied under the influence of both a static and an alternating microwave electric field. It was shown that the shape of a metal nanoobject significantly affects the conformations of adsorbed polyampholytes.

The nature of adsorption of macromolecules on the surface of a nanoobject is also greatly influenced by its chemical composition and structure, which is especially important when considering quantum dots of various chemical compositions. In addition, when semiconductor quantum dots are placed in an external electric field, the values of the surface density of induced charges will be lower than for metal nanoparticles [22]. This is especially important when considering complexes consisting of semiconductor and metal nanoparticles with polyelectrolyte macromolecules adsorbed on them.

It was previously noted in [21] that the frequency dependence of the dipole polarizability of metal nanoparticles located in a microwave (in the traditional technical classification, but at the same time, low-frequency compared to the infrared frequency range) electric field practically does not manifest itself. However, it becomes noticeable in the case of nanoparticles made from materials with a sufficiently low specific conductivity, for example, from pure or lightly doped semiconductors such as germanium.

Therefore, the purpose of this work is a more detailed study of changes in the conformations of polyampholytic macromolecules adsorbed on the surface of semiconductor spheroidal nanoparticles in an alternating microwave electric field. As well as the generalization of the mathematical model of the formation of a quasi-equilibrium macrochain layer [21] to the case of the dispersion dependence of the permittivity of the material of a conducting nanoparticle of a more general form, including the presence of a real part. In particular, the construction of a new version of the theoretical model with going beyond the quasi-static approximation, that is, taking into account the effects of delay, the manifestation of which will be the more noticeable, the more extended the considered structures are on the scale of electromagnetic wavelengths.

2. General mathematical model of the macrochain layer of a nanospheroid in an external low-frequency field

2.1 Formation of a quasi-equilibrium conformational structure of polyelectrolyte chain links adsorbed on a nanospheroid with low electrical conductivity polarized in an external harmonically variable electric field at a frequency significantly lower than the plasma frequency of the material (undoped semiconductor) of the nanoparticle.

A polyelectrolyte macrochain adsorbed on the surface of a spheroidal nanoparticle in the simplest approximation can be considered as an ideal Gaussian chain [19] interacting with an electrically neutral adsorbent particle through van der Waals forces, and in the case of a charged or polarized nanoparticle, Coulomb forces, or forces of the "charge- dipole" [19].

The conformational function $\psi(\mathbf{r})$, which depends on the radius vector $\mathbf{r}$ of a chain link and takes into account the entropy factor for the formation of the bulk structure of a macromolecule, can be calculated on the basis of a specialized differential equation [23], which was previously done in the case of a short-range adsorbing potential [17, 19]. When applying an external, harmonically changing electric field $E_0 \exp(-i\omega t)$, at a sufficiently small value of the frequency ω, it is possible to use the quasi-stationary approximation. It is obvious that the frequency ω, in this case, should be less than the frequency of the characteristic rose mode of the macrochain. Under such conditions, it is reasonable to consider quasi-equilibrium conformations of a polymer molecule adsorbed on a nanoparticle in an external field. In a simple approach, taking into account the interaction of macrochain links with the field of a charged and polarized nanoparticle reduces to introducing the Boltzmann factor W [19, 21].

When a spheroidal nanoparticle is placed in a quasi-stationary uniform electric field of strength $\mathbf{E}_0$, an additional field of a polarized particle arises. To describe the field of charged and/or polarized ellipsoids of revolution (half axes $a = b \neq c$), spheroidal coordinates $\xi = (r_1 + r_2)^2 / 4 - a^2$, $\eta = (r_1 - r_2)^2 / 4 - a^2$, φ [22] are usually used. If the vector $\mathbf{E}_0$ is oriented along the c-axis of the spheroid, the potential $\Phi(\xi, \eta)$ of the external field $\mathbf{E}_0 \mathbf{r}$, together with the potentials $\varphi_Q(\xi)$ and $\varphi_P(\xi, \eta)$ fields of the charged and polarized spheroid, can be written as [21]

$$\Phi(\xi, \eta) = -\mathbf{E}_0 \mathbf{r} + \varphi_Q(\xi) + \varphi_P(\xi, \eta). \tag{1}$$

With a harmonic change in the quasi-stationary field with a frequency ω, the semiconductor material of the nanoparticle is characterized by a complex-valued permittivity $\varepsilon(\omega)$. The potential $\varphi^{(e)}(\xi, \eta) = -\mathbf{E}_0 \mathbf{r} + \varphi_P(\xi, \eta)$ of the resulting field in space outside a conducting uncharged spheroid polarized in an alternating external uniform field parallel to its symmetry axis z can be written in the following form (without the phase factor $\exp(-i\omega t)$) [21]

$$\varphi^{(e)}(\xi,\eta) = \varphi_0(\xi,\eta) \left\{ 1 - \frac{[\varepsilon(\omega) - \varepsilon^{(e)}]a^2 c}{\left\{ \varepsilon^{(e)} + [\varepsilon(\omega) - \varepsilon^{(e)}]n^{(z)} \right\}} \int_{\xi}^{\infty} \frac{d\xi'}{\left(\xi' + c^2\right)^{3/2}\left(\xi' + a^2\right)} \right\}. \qquad (2)$$

$$n^{(z)} = \frac{1 + e^2}{e^3}\left(e - \text{arctg}\, e \right), \quad \varphi_0(\xi,\eta) = -E_0 z = -E_0 \left[\frac{(\xi + c^2)(\eta + c^2)}{c^2 - a^2} \right]^{1/2}. \qquad (3)$$

The constant $\varepsilon^{(e)}$ in (2) is the permittivity of the solvent.

Far from the surface of an uncharged spheroid, the potential of the resulting field includes the characteristic field of an induced electric dipole with polarizability $\alpha^{(j)}(\omega)$

$$\varphi^{(e)}(\mathbf{r}) = -\mathbf{E}_0 \mathbf{r} + \alpha^{(j)}(\omega)\mathbf{E}_0 \mathbf{r} / r^3. \qquad (4)$$

The dipole dynamic polarizability $\alpha^{(j)}(\omega)$ of a spheroid is a tensor of the second rank, which in the system of its principal axes takes the form

$$\alpha^{(j)}(\omega) = \frac{a^2 c}{3} \frac{\varepsilon(\omega) - \varepsilon^{(e)}}{\varepsilon^{(e)} + \left[\varepsilon(\omega) - \varepsilon^{(e)} \right] n^{(j)}}, \quad j = x, y, z. \qquad (5)$$

Here, in (5) $n^{(j)}$ are the depolarization coefficients of the spheroid, and $n^{(x)} = n^{(y)} = \frac{1}{2}\left[1 - n^{(z)} \right]$. The frequency dependence of the permittivity $\varepsilon(\omega)$ of the semiconductor material of the nanoparticle is represented by the generalized Drude-Lorenz model [24]

$$\varepsilon(\omega) = \varepsilon_\infty - \frac{\omega_p^2}{\omega^2 + i\omega\gamma}, \qquad (6)$$

where ω_p, γ - plasma frequency and frequency of collisions of conduction electrons, respectively; ε_∞ - constant high-frequency part of the permittivity, introduced in connection with the need to take into account interband transitions in a semiconductor. As noted in [21], at frequencies ω_p much lower than the plasma frequency, the polarizability factor

$$\frac{[\varepsilon(\omega) - \varepsilon^{(e)}]a^2 c}{\left\{ \varepsilon^{(e)} + [\varepsilon(\omega) - \varepsilon^{(e)}]n^{(z)} \right\}}$$

standing in front of the integral on the right side of (2), weakly depends on the frequency. For a more detailed analysis of this dependence in the region of "conformational resonance" of the macrochain, i.e., for frequencies of the order of 10^9-10^{10} Hz, we use the formula for the limiting transition from the permittivity (6) to an expression containing the specific conductivity $\sigma = const$ of the semiconductor $\varepsilon = const$ without taking into account its frequency dispersion [22]

$$\varepsilon(\omega) \underset{\omega \ll \omega_p}{\longrightarrow} \varepsilon + i\frac{4\pi\sigma}{\omega}. \qquad (8)$$

Note that this expression follows from the Maxwell equation in the absence of dispersion ($\sigma = const$, $\varepsilon = const$)

$$\text{rot}\,\mathbf{H} = \frac{4\pi\sigma}{c}\mathbf{E} + \frac{\varepsilon}{c}\frac{\partial}{\partial t}\mathbf{E}, \qquad (9)$$

with a harmonic change in the electric and magnetic fields

$$\mathbf{E}(t) = \mathbf{E}_0 \exp(-i\omega t), \quad \mathbf{H}(t) = \mathbf{H}_0 \exp(-i\omega t).$$

Then, taking into account (8), and if the frequencies are such that $\omega \ll \gamma$, we obtain for the conductivity

.

$$\sigma = \frac{\omega_p^2}{4\pi\gamma} . \tag{10}$$

2.2 Spherical nanoparticle

The depolarization coefficients of a spherical nanoparticle $n^{(j)} = 1/3$ are the same for all three values of j, and then for the dipole dynamic electric polarizability $\alpha_s(\omega)$ of a conducting spherical particle of radius R for subplasma frequencies $\omega \ll \omega_p$ we obtain

$$\alpha_s(\omega) = \frac{\varepsilon(\omega) - \varepsilon^{(e)}}{\varepsilon(\omega) + 2\varepsilon^{(e)}} R^3 \rightarrow \frac{i4\pi\sigma - \omega\left(\varepsilon^{(e)} - \varepsilon\right)}{i4\pi\sigma + \omega\left(2\varepsilon^{(e)} + \varepsilon\right)} R^3 . \tag{11}$$

In this case, the real and imaginary parts of the dipole polarizability can be written as

$$\alpha_s'(\omega) = \frac{(4\pi\sigma)^2 - \omega^2(\varepsilon^{(e)} - \varepsilon)(2\varepsilon^{(e)} + \varepsilon)}{(4\pi\sigma)^2 + \omega^2(2\varepsilon^{(e)} + \varepsilon)^2} R^3 , \tag{12}$$

$$\alpha_s''(\omega) = \frac{12\pi\sigma\omega\varepsilon^{(e)}}{(4\pi\sigma)^2 + \omega^2(2\varepsilon^{(e)} + \varepsilon)^2} R^3 . \tag{13}$$

It follows from (12) that the sign of the polarization of the nanoparticle switches at the frequency $\omega = \omega_0$, and then for the characteristic switching frequency ω_0 we obtain the expression

$$\omega_0 = \left(4\pi / \sqrt{(\varepsilon^{(e)} - \varepsilon)(2\varepsilon^{(e)} + \varepsilon)}\right)\sigma .$$

In the limit of very low frequencies $\omega \rightarrow 0$, from (12) and (13) the following expressions follow:

$$\lim_{\omega \rightarrow 0} \alpha_s'(\omega) = \left[1 - \frac{3\varepsilon^{(e)}(2\varepsilon^{(e)} + \varepsilon)}{(4\pi\sigma)^2}\omega^2\right]R^3 , \tag{14}$$

$$\lim_{\omega \rightarrow 0} \alpha_s''(\omega) = \frac{3\varepsilon^{(e)}\omega}{4\pi\sigma} R^3 . \tag{15}$$

It should also be noted that the parameter $\varepsilon = \text{const}$ is not present at all in formula (15) for the imaginary part of the polarizability; therefore, the result (15) coincides with the corresponding expression obtained in [21] for metal nanoparticles.

From (12) it follows that all possible values $\alpha_s'(\omega)/R^3$ of the real part of the polarizability belong to the interval [-b, 1], where the constant b is determined by the expression

$$b = \frac{(\varepsilon^{(e)} - \varepsilon)}{(2\varepsilon^{(e)} + \varepsilon)} . \tag{16}$$

An imaginary part $\alpha_s''(\omega)$ of the polarizability determines not only the dissipation of the energy of the external electromagnetic field in the nanoparticle [21], but also the amplitude of oscillations of the cross part of the induced dipole moment $\alpha_s''(\omega)E_0 \exp(-i\omega t + i\pi/2)$. In this case, the oscillations of the corresponding dipole component of the field themselves are shifted in phase by an amount $\pi/2$ relative to the oscillations of the external field $E_0 \exp(-i\omega t)$. Oscillations of the real part of the polarizability $\alpha_s'(\omega)E_0 \exp(-i\omega t)$ will be in-phase with the external seed field, as well as the oscillations of the secondary in-phase field corresponding to it, that is, the field of the in-phase oscillating induced dipole moment.

Note that expressions (11) and (12-13) can be obtained not only by using the limit transition (8), but also by solving the equations for the field inside and outside the conducting nanoparticle, followed by matching the obtained solutions on the boundary sphere of radius *R*.

2.3 Spheroidal nanoparticle

In the case of a spheroidal nanoparticle, for the components of the diagonalized polarizability tensor $\alpha^{(j)}(\omega)$, from (5) and (8) we obtain

$$\alpha^{(j)}(\omega) = \frac{abc}{3} \frac{i4\pi\sigma - \omega(\varepsilon^{(e)} - \varepsilon)}{\omega\varepsilon^{(e)} + \left[i4\pi\sigma - \omega(\varepsilon^{(e)} - \varepsilon)\right]n^{(j)}}, \quad j = x, y, z \,. \tag{17}$$

For the corresponding (17) real and imaginary parts of the spheroid polarizability tensor $\alpha^{(j)}(\omega)$, we can write

$$\alpha'^{(j)}(\omega) = \frac{abc}{3} \frac{(4\pi\sigma)^2 n^{(j)} - \omega^2(\varepsilon^{(e)} - \varepsilon)\left[\varepsilon^{(e)}(1 - n^{(j)}) + \varepsilon n^{(j)}\right]}{\left[4\pi\sigma n^{(j)}\right]^2 + \omega^2\left[\varepsilon^{(e)}(1 - n^{(j)}) + \varepsilon n^{(j)}\right]^2} \,. \tag{18}$$

$$\alpha''^{(j)}(\omega) = \frac{abc}{3} \frac{4\pi\sigma\omega\varepsilon^{(e)}}{\left[4\pi\sigma n^{(j)}\right]^2 + \omega^2\left[\varepsilon^{(e)}(1 - n^{(j)}) + \varepsilon n^{(j)}\right]^2} \,. \tag{19}$$

Then the real part of the potential (2) of the resulting field outside the nanoparticle

$$\operatorname{Re}\varphi^{(e)}(\xi,\eta;t) = \varphi_0(\xi,\eta) \times \cos\omega t$$

$$\times\left\{1 - \frac{(4\pi\sigma)^2 n^{(j)} - \omega^2(\varepsilon^{(e)} - \varepsilon)\left[\varepsilon^{(e)}(1 - n^{(j)}) + \varepsilon n^{(j)}\right]}{\left[4\pi\sigma n^{(j)}\right]^2 + \omega^2\left[\varepsilon^{(e)}(1 - n^{(j)}) + \varepsilon n^{(j)}\right]^2} a^2 c \int_{\xi}^{\infty} \frac{d\xi'}{\left(\xi' + c^2\right)^{3/2}\left(\xi' + a^2\right)}\right\} \,. \tag{2'}$$

The oscillations of the corresponding dipole component of the field, shifted in phase by an amount $\pi/2$ relative to the oscillations of the external field $E_0 \exp(-i\omega t)$, are determined by the imaginary part of the potential (2) and, accordingly, the imaginary part of the polarizability $\alpha''(\omega)$

$$\operatorname{Im}\varphi^{(e)}(\xi,\eta;t) = \varphi_0(\xi,\eta) \cdot \sin\omega t \times$$

$$\times\frac{4\pi\sigma\omega\varepsilon^{(e)} a^2 c}{\left[4\pi\sigma n^{(j)}\right]^2 + \omega^2\left[\varepsilon^{(e)}(1 - n^{(j)}) + \varepsilon n^{(j)}\right]^2} \int_{\xi}^{\infty} \frac{d\xi'}{\left(\xi' + c^2\right)^{3/2}\left(\xi' + a^2\right)} \,. \tag{2''}$$

For the frequency ω_0 of polarization sign switching in this case, it follows from (18) that

$$\omega_0 = 4\pi\sigma \sqrt{\frac{n^{(j)}}{(\varepsilon^{(e)} - \varepsilon)\left[\varepsilon^{(e)}(1 - n^{(j)}) + \varepsilon n^{(j)}\right]}} \,, \tag{20}$$

whence at $n^{(j)} = 1/3$ follows the previously obtained value of the frequency ω_0 of switching the polarization sign for the ball $\omega_0 = 4\pi\sigma / \sqrt{(\varepsilon^{(e)} - \varepsilon)(2\varepsilon^{(e)} + \varepsilon)}$.

.

The numerical estimates of $\alpha'_s(\omega)/R^3$ and $\alpha'^{(z)}(\omega)/(a^2c)$ in the frequency range of "conformational resonance" carried out in [21], i.e., $\sim 10^9$-10^{10} Hz, performed at $\varepsilon=0$ for spherical or spheroidal nanoparticles of metals such as Ag or Au ($4\pi\sigma \sim 10^{16} \div 10^{17}$ Hz) showed that the specific polarizabilities are close to 1. The frequency dependences of the polarizabilities $\alpha_s(\omega)$ and $\alpha^{(j)}(\omega)$ pure or lightly doped semiconductors of the Ge type are more noticeable , since their conductivity is $4\pi\sigma \sim 10^9 \div 10^{10}$ Hz, i.e. of the same order as the frequencies ω of the external field.

In the case of an excess charge Q on the spheroid in the outer region outside it, an additional quasi-static field with a potential $\varphi_Q(\xi)$ arises [21, 22], and then the interaction energy of the resulting electric field with a group of polyelectrolyte units bearing a characteristic charge q' takes the form:

$$V_{tot}(\xi,\eta) = q'\varphi_Q(\xi) + q'\varphi^{(e)}(\xi,\eta) .$$ (21)

Then the probability of detecting a polymer link at a point with coordinates ξ,η above the nanoparticle surface in the equilibrium configuration of polyelectrolyte macrochains at temperature T is determined by the Boltzmann factor $W(\xi,\eta)$ based on the potential (21)

$$W(\xi,\eta) = \exp\left\{ -\frac{q'}{kT}\left[\varphi_Q(\xi) + \varphi^{(e)}(\xi,\eta)\right] \right\}.$$ (22)

The Boltzmann factor (22) contains all the information about the interaction of a polymer with an electric field. Upon adsorption of a macrochain on an elongated or compressed spheroidal nanoparticle polarized in an external field, the formation of edge layer conformations within the model of unbound units was studied in [21]. In this case, the contribution of the quasi-stationary field (21) to the appearance of equilibrium conformations of the macromolecule is taken into account by means of the Boltzmann factor. The final spatial distribution of the density $n(\xi,\eta)$ of units of a polyelectrolyte macrochain adsorbed by a polarized nanospheroid takes the form

$$n(\xi,\eta) = \psi^2(\xi,\eta)\exp\left[-\frac{V_{tot}(\xi,\eta)}{kT} \right].$$ (23)

Thus, the equilibrium density distribution of chain links (23) contains two factors: entropy $\psi^2(\xi,\eta)$, which contains the memory of the linear structure of the macrochain and details of the surface relief of the adsorbing nanoparticle [21], and Boltzmann $W(\xi,\eta)$. The conformational functions $\psi^2(\xi,\eta)$ for the entropy factor on the surface of an oblate spheroid were calculated earlier.

2.4 Accounting for the delay effect

Consideration of delay effects becomes necessary when the major semiaxis of the prolate spheroid becomes commensurate in magnitude with the wavelength of the alternating field, i.e. the spheroid becomes sufficiently extended. At the same time, going beyond the quasi-stationary approximation to determine the characteristics of an alternating electric field, that is, taking into account the delay effect due to the finiteness of the speed of light, is associated with the need to solve the Helmholtz equation instead of the Laplace equation. Obviously, even for the case of a spherical particle, the analytical solution of the problem is associated with significant difficulties. Such a problem for a ball has already been solved earlier in the theory of diffraction and is known as the Mie solution [24]. A harmonically changing electromagnetic field can be either a standing or traveling wave. Mi's solution is written for the latter.

If a plane linearly polarized electromagnetic wave propagates along the polar z-axis of a spherical coordinate system (SCS) r,θ,ϕ , the electric field is directed along the x-axis, and the magnetic field is directed along the y-axis, then the Cartesian components of the strengths of these fields

$$E_x^0 = H_y^0 = \exp(ikz) = \exp(ikr\cos\theta) = \sum_{n=0}^{\infty}(2n+1)i^n\sqrt{\frac{\pi}{2kr}}J_{n+1/2}(kr)$$

as well as the components in the SSC, written in terms of the U, U' Borgnies potentials

$$E_r = \frac{\partial^2 U}{\partial r^2} + k^2 U, \quad E_\theta = \frac{1}{r}\frac{\partial^2 U}{\partial r\partial \theta}, \quad E_\phi = -\frac{i\omega\mu}{\varepsilon r}\frac{\partial U'}{\partial \theta}.$$

$$H_r = \frac{\partial^2 U'}{\partial r^2} + k^2 U', \quad H_\theta = \frac{1}{r}\frac{\partial^2 U'}{\partial r\partial \theta}, \quad H_\phi = \frac{ik^2 c}{\omega\mu r}\frac{\partial U}{\partial \theta}.$$

The boundary conditions on the surface of the ball have the form

$$\left.\begin{aligned}
\frac{\partial}{\partial r}(ru_2) &= \frac{\partial}{\partial r}(ru_1), & \frac{k_1^2 u_1}{\mu_1} &= \frac{k_2^2 u_2}{\mu_2} \\[2mm]
\frac{\partial}{\partial r}(rv_2) &= \frac{\partial}{\partial r}(rv_1), & \mu_1 v_1 &= \mu_2 v_2
\end{aligned}\right\}, \quad r = R.$$

$$k_j^2 = \frac{\varepsilon_j \mu_j \omega^2}{c^2} + i\frac{4\pi\sigma_j \mu_j \omega}{c^2}.$$

The functions $u=U/r$, $v=U'/r$ of the Borgnis potentials U,U' are defined by the expressions [25]

$$u = \begin{cases}
\displaystyle\sum_{n=0}^{\infty} a_n\left[\psi_n(k_1 r) + \alpha_n \varsigma_n^{(1)}(k_1 r)\right]\left[-\frac{d}{d\theta}P_n(\cos\theta)\right]\cos\phi, & r > R \\[4mm]
\displaystyle\sum_{n=0}^{\infty} A_n \psi_n(k_2 r)\left[-\frac{d}{d\theta}P_n(\cos\theta)\right]\cos\phi, & r < R
\end{cases}$$

Here the constant coefficients

$$a_n = \frac{2n+1}{n(n+1)}\frac{i^{n-1}}{k}, \quad \alpha_n = \frac{(k_1^2/\mu_1)\psi_n(k_1 R)\Psi_n(k_2 R) - (k_2^2/\mu_2)\psi_n(k_2 R)\Psi_n(k_1 R)}{\Delta},$$

$$A_n = \frac{k_1^2\left[\Psi_n(k_1 R)Z_n^{(1)}(k_1 R) - \psi_n(k_1 R)\varsigma_n^{(1)}(k_1 R)\right]}{\mu_1\Delta}$$

are specified on the surface of a spherical nanoparticle, and the functions

$$\Psi_n(x) = \frac{d}{dx}\left[x\cdot\psi_n(x)\right], \quad \psi_n(x) = \sqrt{\frac{\pi}{2x}}J_{n+1/2}(x), \quad \varsigma_n^{(1)}(x) = \sqrt{\frac{\pi}{2x}}H_{n+1/2}^{(1)}(x),$$

$$Z_n^{(1)}(x) = \frac{d}{dx}\left[x\cdot\varsigma_n^{(1)}(x)\right], \quad \Delta = \frac{k_2^2}{\mu_2}Z_n^{(1)}(k_1 R)\psi_n(k_2 R) - \frac{k_1^2}{\mu_1}\Psi_n(k_2 R)\varsigma_n^{(1)}(k_1 R).$$

are based on the well-known Bessel functions $J_{n+1/2}(x)$ and Hankel functions of the first kind $H_{n+1/2}^{(1)}(x)$ of a half-integer index. The expressions for the coefficients β_n and B_n that define the function $v=U'/r$ have a similar form [25]. The numerical implementation of the model even for spherical nanoparticles is very laborious, but it may become necessary if the field quasi-stationarity condition is violated.

To form a conformation map of the polyelectrolyte chain, information is required on the radial-angular dependences of the components of the electric field vector $\mathbf{E(r)}$: $E_r(r,\theta,\phi)$, $E_\theta(r,\theta,\phi)$, $E_\phi(r,\theta,\phi)$. The azimuthal component of the field $E_\phi(\mathbf{r})$, which was absent in the quasi-stationary approximation and the corresponding axially symmetric field, appears due to the magnetic components $H_j(\mathbf{r})$ and reflects their inclusion in the general case of the electromagnetic field. The potential energy of interaction of polyelectrolyte units $\mathbf{E(r)}$ with the field instead of formula (21) will then be determined by the expression

$$V_{tot}(\mathbf{r}) = q'\varphi_Q(\mathbf{r}) - q'\int\mathbf{E(r)}\cdot d\mathbf{r}. \tag{24}$$

In the case of polyampholyte, with an electric dipole moment $\mathbf{p}$ of the link, this energy takes the form $V_{tot}(\mathbf{r}) = \mathbf{p}\nabla\varphi_Q(\mathbf{r}) - \mathbf{p}\mathbf{E}(\mathbf{r})$. The spatial distribution of the unit density $n(\xi,\eta)$ of a polyelectrolyte macrochain adsorbed by a polarized nanospheroid, taking into account the delay effects, will be given, as before, by formula (23), but with the interaction energy $V_{tot}(\mathbf{r})$ defined by formula (24).

3. Molecular dynamics simulation

Molecular dynamics (MD) simulation of polyampholytic polypeptides on the surface of a spherical germanium nanoparticle was performed using the NAMD 2.14 software package [26]. A model of a germanium nanoparticle was obtained by cutting a ball with a radius of 2.4 nm from a germanium crystal, and its atoms remained fixed during the simulation. Three generally neutral polyampholytic polypeptides have been considered:

1) **P1** polypeptide consisting of 400 amino acid residues with 320 Ala units with evenly distributed 40 Asp units (D, charge -1e) and 40 Arg units (R, charge +1e) – $(A_2DA_4RA_2)_{40}$;

2) **P2** polypeptide – $(A_4R_2A_8D_2A_4)_{20}$;

3) **P3** polypeptide – $A_8(A_8D_2A_{16}R_2A_8)_{11}A_8$.

For polypeptides, the CHARMM36 force field was used [27-28]. Non-covalent interactions with a germanium nanoparticle were described by the Lennard-Jones potential parameterized in the UFF force field [29]. This force field is widely used in the study of various molecular systems by the MD, including the study of the adsorption of molecules on various solid surfaces [30-31]. The van der Waals potential was cut off at a distance of 1.2 nm using a smoothing function between 1.0 and 1.2 nm. Electrostatic interactions were calculated directly at a distance of 1.2 nm, and at a larger distance, the Ewald particle-grid method (PME) [32] was used with a grid step of 0.11 nm. The entire nanosystem was placed in a cube with 22 nm edges filled with TIP3P water molecules [33].

First, modeling of polyampholytic polypeptides was carried out on the surface of a non-polarized germanium nanoparticle. The resulting conformational structures of polypeptides were used as starting points for modeling on the surface of a germanium nanoparticle polarized in an external static or alternating electric field. In total, three starting conformations were obtained for each considered polypeptide. In an external uniform electric field on the surface of a spherical semiconductor nanoparticle, charges are distributed with surface density σ_p proportional to the cosine of the angle θ between the direction of the electric field vector $\mathbf{E}$ and the normal to the nanoparticle surface [22, 34]:

$$\sigma_p = \frac{3p}{4\pi r}\cos\theta \ , \tag{25}$$

where p is the dipole moment of the ball and r is its radius.

Therefore, the polarization of a germanium nanoparticle was specified through a change in the partial charges of atoms on its surface according to the cosine law of the orientation angle of the normal [35]. The following peak values of the induced dipole moment of a spherical germanium nanoparticle were considered: $p_1 \approx 3.7$, $p_2 \approx 7.4$ и $p_3 \approx 14.8$ kD. In this case, at the positively charged pole of the nanoparticle, the atoms acquired partial charges induced by the electric field equal approximately to +0.1e, +0.2e, and +0.4e. In the case of static polarization of a germanium nanoparticle, MD simulation was performed at a constant temperature (Berendsen thermostat) at 900 K followed by a decrease to 300 K. This made it possible to reach deeper minima of the conformational energy of the macrochain, including in a shorter section of the trajectory [14, 17-18, 19-20]. At the same time, to control the obtaining of equilibrium conformations, the change in the mean square distance between polypeptide atoms in different conformations (RMSD) was monitored.

In addition, we considered the case when, in the course of MD simulation, the densities of induced charges on the surface of a germanium nanoparticle periodically changed in time according to the sine law with an oscillation period $T = 2.4$ ns during 4 oscillation periods. Each oscillation period was divided into 8 equal time segments of 0.3 ns each, during which the field did not change, and the value of the dipole moment of the nanoparticle in the selected segment was set by averaging it over the entire length of the segment. The dipole moment of the nanoparticle changed in the following sequence, starting from the starting conformation of the polypeptide: +0.69p (mean value in the range of oscillations from $\pi/8$ to $3\pi/8$), +0.97p (from $3\pi/8$ to $5\pi/8$), +0.69p (from $5\pi/8$ to $7\pi/8$), 0 (from $7\pi/8$ to $9\pi/8$), -0.69p (from $9\pi/8$ to $11\pi/8$), -0.97p (from $11\pi/8$ to $13\pi/8$) , -0.69p (from $13\pi/8$ to $15\pi/8$), 0 (from $15\pi/8$ to $17\pi/8$). MD simulation with a

periodic change in the polarity of a germanium nanoparticle was performed at constant temperatures of 300 and 900 K [15-16, 20].

Based on the simulation results, the resulting conformations were used to calculate the radial distributions of the density of polypeptide atoms and the distributions of the linear density of polypeptide atoms along the polarization axis. The angular distributions of polypeptide atoms were also calculated.

4. Results of MD simulation

4.1 Rearrangement of the conformational structure of polyampholytic polypeptides upon static polarization of a germanium spherical nanoparticle

Figure 1a shows the conformation of the P1 polypeptide on the surface of a germanium spherical nanoparticle, obtained from the results of MD simulation on the surface of a non-polarized nanoparticle. Both the P1 polypeptide macromolecule (Fig. 1a) and the P2 and P3 polypeptides completely envelop the non-polarized germanium nanoparticle. These conformations of polypeptides were used as starting points in modeling on the surface of a polarized germanium nanoparticle, including with a periodic change in its polarity. Figure 2a shows the curves of radial distributions of the average density of atoms of the P1 polypeptide with differentiation according to the types of units. They have a peak at the surface of a nanoparticle, which is characteristic of the adsorption of macromolecules on the neutral surface of solid adsorbents of various shapes [14, 18]. Figure 3a shows the distributions of the average linear density of P1 polypeptide atoms on the surface of a non-polarized germanium nanoparticle. It can be seen that, on the whole, the atoms of the macrochain are distributed uniformly along the z axis (coinciding with the polarization axis of the nanoparticle upon further consideration).

a   b   c
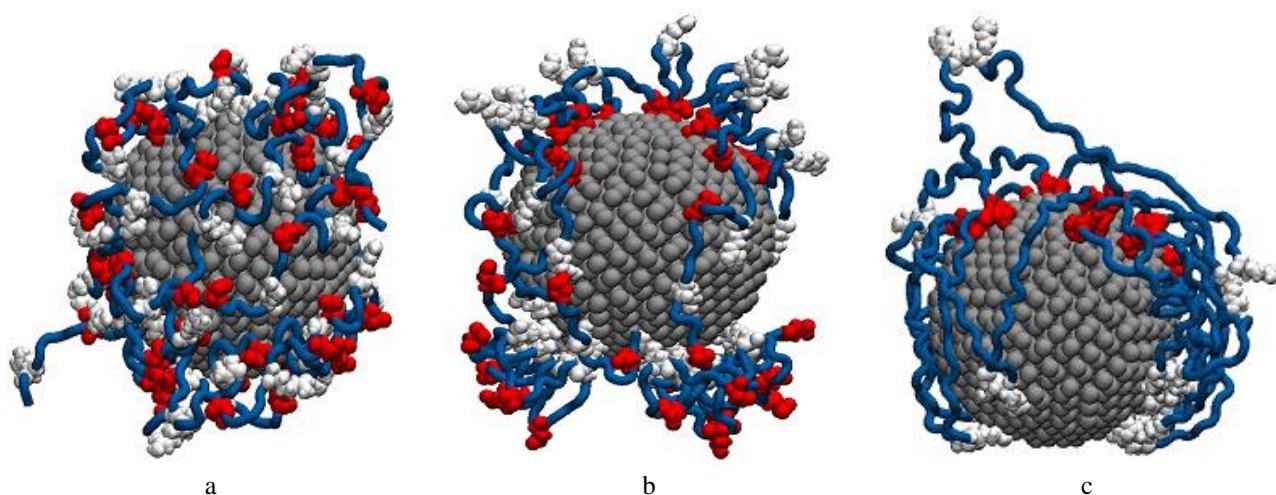
Fig.1 The conformational structure of polypeptides P1 (b) and P3 (c) at the end of MD simulation on the surface of a polarized germanium nanoparticle (the dipole moment is directed from bottom to top), as well as the starting conformation of the polypeptide P1 (a) on the surface of a non-polarized nanoparticle (blue tube - Ala units, Asp units are shown in red, Arg units are shown in white, germanium nanoparticles are shown in gray).

As the dipole moment of the germanium spherical nanoparticle increased, the conformational structure of the adsorbed polyampholyte changed due to the shift of charged amino acid residues to oppositely charged subpolar regions of the nanoparticle (Figs. 1b and 1c). For polypeptides P1 (Fig. 1b) and P2, in which the number of neutral units between the charged ones was less than that of the P3 polypeptide, the formation of a significant number of macrochain loops was observed on the surface of the polarized nanoparticle. They were stretched along the polarization axis of the nanoparticle, which led to the stretching of the macromolecular fringe. Such rearrangement began to occur from the value of the dipole moment equal to p_2 and higher. For the P3 polypeptide, the number of macrochain loops extended along the polarization axis from the surface of the nanoparticle was small. In this case, the charged amino acid residues Arg and Asp adsorbed at the poles of the polarized nanoparticle were linked by a fragment consisting of neutral Ala units located in the central region of the nanoparticle (Fig. 1c).

Previously, in [14], during MD simulation on the surface of a polarized spherical gold nanoparticle, a similar pattern of rearrangement of polyampholytic polypeptides with the same sequence of links was observed. However, in contrast to the germanium nanoparticle, such conformational changes began to occur at a surface charge density at the poles much higher than for the germanium nanoparticle: the charge of atoms at the pole on the gold nanoparticle was $0.5e$, while on the germanium nanoparticle it was only $0.2e$. This is due to the fact that the considered Lennard-Jones potential, which describes van der Waals interactions, was lower for germanium than for gold. In addition, the radius of the gold nanoparticle was smaller (1.5 nm), but the dipole moments of the nanoparticles were approximately the same: 5.5 kD for gold and 7.4 kD for germanium nanoparticles.

Such a rearrangement of the conformational structure of polyampholytic polypeptides on the surface of a polarized spherical germanium nanoparticle led to a change in the radial distributions of the average density of macrochain atoms (Fig. 2b). It can be seen that, compared with the distribution on a non-polarized nanoparticle (Fig. 2a), there was a decrease and broadening of the profile of the radial distribution over all atoms of the polypeptide. In this case, the charged units of Arg and Asp are mainly concentrated near the surface of the nanoparticle (Fig. 2b), which is associated with their adsorption at the poles of the germanium nanoparticle, while the neutral units of Ala are far from the surface. On the whole, the radial distributions of the mean atomic density of polyampholyte polypeptides on the surface of a polarized germanium nanoparticle turned out to be similar to the radial distributions of the atomic density of polyampholytes obtained for a polarized gold nanoparticle.
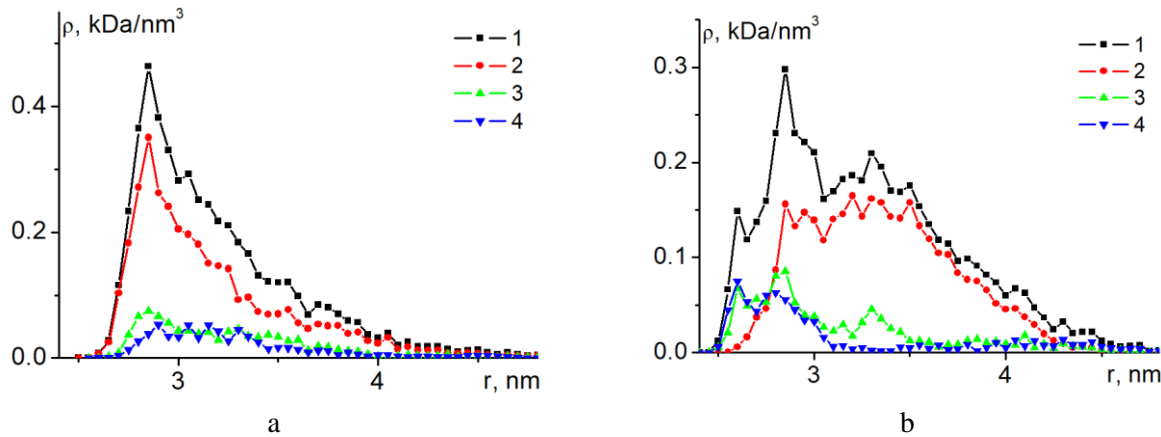
Fig.2 Radial dependences of the average density of atoms of the P1 polypeptide with differentiation according to the types of links in the starting conformation on the surface of a non-polarized spherical nanoparticle (a), as well as at the end of MD simulation on the surface of a germanium nanoparticle polarized with a dipole moment p_3 (b) (1 - for all atoms of the polypeptide; 2, 3 and 4 - for Ala, Arg and Asp links, respectively).
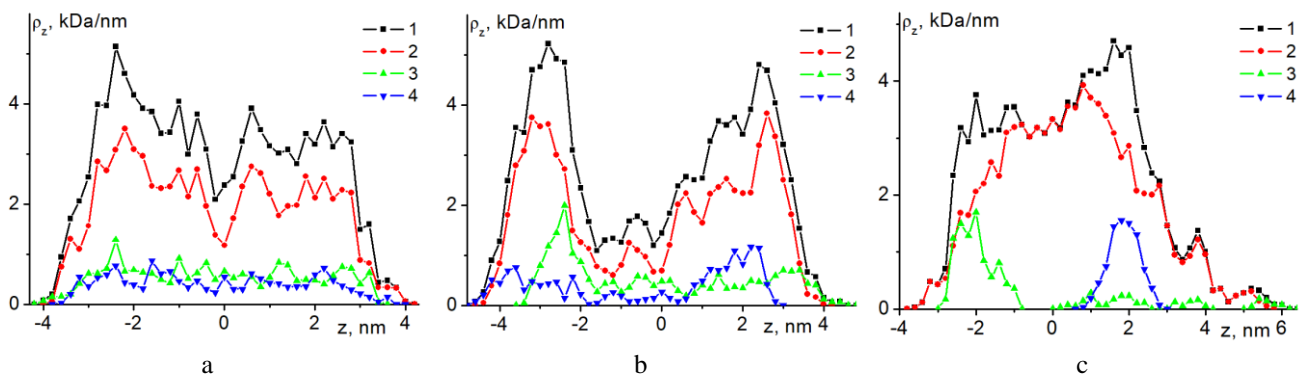
Fig.3 Distributions of the average linear density of atoms of the P1 polypeptide in the starting conformation (a), as well as of the polypeptides P1 (b) and P3 (c) at the end of the MD simulation on the surface of a spherical germanium nanoparticle polarized with a dipole moment p_3 (1 – over all atoms of the polypeptide; 2, 3 and 4 - for links Ala, Arg and Asp, respectively).

The distributions of the average linear density of polypeptide atoms along the nanoparticle polarization axis were also plotted (Fig. 3). On the surface of non-polarized spherical germanium nanoparticle, the links were generally distributed uniformly along the z axis of the nanoparticle directed along the polarization axis (Fig. 3a). On the surface of the polarized nanoparticle for polypeptides P1 (Fig. 3b) and P2, there was a significant change in the distribution profile of the average linear density of macrochain atoms with the appearance of peaks near the poles of the nanoparticle. This indicates a shift of the macrochain links to the subpolar regions of the nanoparticle. For the P3 polypeptide (Fig. 3c), mainly charged units were concentrated at the poles of the polarized germanium nanoparticle. At the same time, neutral amino acid residues Ala connected them, being located mainly in the central region of the nanoparticle (Fig. 1c).

4.2 Rearrangement of the conformational structure of polyampholytic polypeptides upon periodic change in the polarity of a germanium spherical nanoparticle

In the MD simulation of polyampholytic polypeptides on the surface of a germanium nanoparticle with a periodic change in its polarity over time at a temperature of 300 K and the peak value of the p_2 nanoparticle dipole moment, the macrochain units shifted to the equatorial region of the nanoparticle (Fig. 4). This is due to the fact that, upon polarization reversal of the nanoparticle, charged units of the polyampholyte are displaced from like-charged poles of the nanoparticle to the weakly charged equatorial region of the nanoparticle. They remain there due to the weak local electric field near the equator, held by the van der Waals attraction of the macrochain to the surface. Over time, after several periods of change in the polarity of the nanoparticle, all units of the polyampholyte shifted to its equatorial region.

a   b
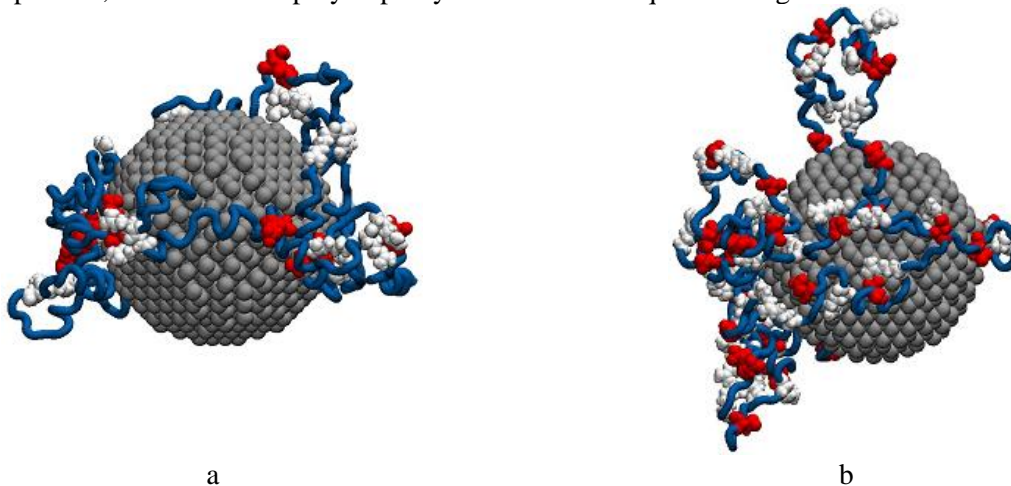
Fig.4 Conformational structures of polypeptides P3 (a) and P1 (b) at the end of MD modeling at a temperature of 300 K with a periodic change in the polarity of the germanium nanoparticle at the peak value of the dipole moment of the nanoparticle equal to p_2 (blue tube - Ala units, Asp units are shown in red, and white – Arg).

Figure 5a shows the dependences of the angular distributions of atoms over all atoms of the P3 polypeptide and over its charged Arg units. The calculation of the angular distribution was carried out with a step of 10 degrees. The lower (Fig. 1 and Fig. 4) pole corresponds to an angle of 180 degrees, the equatorial region - an angle of 90 degrees, and the upper pole - an angle of 0 degrees. The dependences of the angular distributions of atoms of the adsorbed macrochain were normalized to the amplitude values of the concentration of atoms in the equatorial region, taking into account differences in the surface area of spherical belts bounded by circles of different radii: $N(\theta_1,\theta_2)=n(\theta_1,\theta_2)S(80,90)/S(\theta_1,\theta_2)$, where $S(80,90)$ - area of a spherical belt bounded by angles of 80 and 90 degrees, $N(\theta_1,\theta_2)$ - normalized number of macrochain atoms in a spherical belt, $n(\theta_1,\theta_2)$ - the number of macrochain atoms in the spherical belt, and $S(\theta_1,\theta_2)$ area of a spherical belt bounded by angles θ_1 and θ_2.

It can be seen that, compared with the initial conformational structure (Fig. 5a, curve 1) on the surface of an non-polarized nanoparticle, after modeling with a periodic change in the polarity of the nanoparticle, the angular distribution profile of the P3 polypeptide atoms narrowed and is located in the equatorial region (Fig. 5a, curve 2). It can also be seen that at the time when the dipole moment of the nanoparticle is maximum (Fig. 5a, curve 3), the dependence of the angular distribution of the P3 polypeptide atoms almost

.

did not change. This suggests that, upon repolarization of the nanoparticle, the macrochain remains near the equator.

Figure 5b shows that the profile of the radial distribution of the P2 polypeptide atomic density at the end of the MD simulation with a periodic change in polarity at 300 K and p_2 significantly decreased (curve 2) compared to the initial distribution (curve 1) and almost does not change during the last oscillation period (curve 3). This is due to the displacement of the polyampholyte to the equatorial region of the germanium nanoparticle. This character of the conformational rearrangement of polyampholyte polypeptides turned out to be similar to the conformational changes of polyampholytes on the surface of a gold nanoparticle in a microwave electric field [15].

a   b
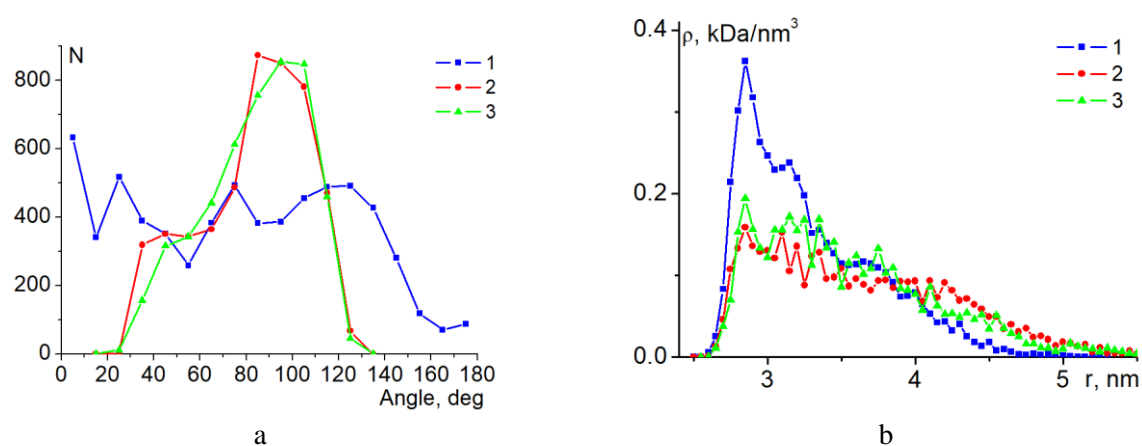
Fig.5 Dependences of the angular distributions of atoms of the polypeptide P3 (a) and the radial distributions of the density of atoms of the polypeptide P2 (b) in the starting conformation (1), at the end of MD simulation (2) with a periodic change in the polarity of the germanium nanoparticle (peak dipole moment p_2) at a temperature of 300 K , as well as at the last simulation period at the time when the dipole moment of the nanoparticle is maximum (3).

In the case of MD simulation of all considered polypeptides on the surface of a germanium nanoparticle with a periodic change in time of its polarity at twice the peak value of the dipole moment of the nanoparticle p_3 and a temperature of 300 K, most of the polyampholyte units were desorbed during the considered time interval. In this case, a small part of the units of the macromolecule remained adsorbed in the equatorial region of the nanoparticle. This was due to the fact that at a higher peak value of the dipole moment of the nanoparticle, stronger changes in the local electric field occurred in its equatorial region, which led to an increase in the displacement amplitude of the charged units. In this case, the forces of attraction of the macrochain to the nanoparticle in the equatorial region were overcome, and most of the amino acid residues of the polyampholyte polypeptide were desorbed.

When modeling at a temperature of 900 K at the peak values of the dipole moment of the p_2 and p_3 nanoparticles, periodic changes in the conformational structure of the adsorbed polyampholytic polypeptide occurred following a change in the polarity of the germanium nanoparticle over time. In this case, potential barriers preventing changes in the conformation of the macrochain were easily overcome due to the high modeling temperature, and the conformational structure of the polyampholyte changed depending on the instantaneous value and direction of the dipole moment of the nanoparticle. Therefore, at the time moments when the dipole moment of the nanoparticle was maximum, the macromolecular fringe assumed an elongated shape, similar to the simulation for static polarization of the nanoparticle (Figs. 1b and 1c).

And at the end of the MD simulation sections, when the dipole moment of the nanoparticle was equal to zero, the polyampholyte shell acquired a shape enveloping the nanoparticle, similar to that shown in Figure 1a. At the same time, both radial and linear distributions of the density of polypeptide atoms at different time points were also similar to the distributions on the surface of a non-polarized (Figs. 2a and 3a) and polarized nanoparticles (Figs. 2b and 3b-c). And the profiles of distributions of the linear density of polypeptide atoms along the polarization axis along the charged amino acid residues Arg and Asp mirrored relative to the equator when the polarity of the nanoparticle was reversed (Figs. 3b and 3c).

4. Conclusion

Thus, a generalization was made of the mathematical model of the formation of a quasi-equilibrium macrochain layer for nanoparticles with low electrical conductivity, which are in an external harmonically varying electric field with a frequency significantly lower than the plasma frequency of the nanoparticle material. With this approach, the permittivity and electrical conductivity of the particle material are simultaneously introduced into consideration. The frequency dependences of the dipole polarizabilities of a sphere and a spheroid manifest themselves most noticeably in the case of semiconductor nanoparticles with an electrical conductivity σ of the order of 10^9-10^{10} Hz, i.e. of the same order of magnitude with the frequencies of the external field. Conductivity of this order is typical for pure or lightly doped semiconductors like Ge. Within the framework of the proposed model, the effect of switching the sign of the nanoparticle polarization upon reaching a certain characteristic frequency of the field, which depends on the conductivity σ of the nanoparticle material, its permittivity, and the depolarization coefficients of the spheroid, was found. It has been shown that adsorption of polymers on lightly doped semiconductor nanoparticles gives rise to the possibility of a more flexible control action on conformational transitions in the macrochain fringe by an alternating electric field of an arbitrarily varied frequency in the range of 10^9-10^{10} Hz. A new version of the theoretical model has been constructed with going beyond the quasi-static approximation, that is, taking into account the delay effects, the manifestation of which is more noticeable for extended nanostructures. The use of this version of the model leads to the appearance of an azimuthal component of the electric field strength, which was absent in the implementation of the quasi-static approximation. This complicates the structure of the resulting field for spheroids with a large long semiaxis.

The performed MD simulation showed that on the surface of a spherical germanium nanoparticle in an external static or alternating electric field of the microwave range, the nature of conformational changes in generally neutral polyampholyte polypeptides with different distribution laws of charged units turned out to be similar to the rearrangement of polyampholyte conformations on the surface of a spherical gold nanoparticle [14-15]. On the surface of a spherical germanium nanoparticle, with an increase in its dipole moment, such a rearrangement of the conformational structure of the polyampholyte occurred, in which part of its charged units shifted to strongly charged subpolar regions. If the distance between oppositely charged units was small compared to the diameter of the nanoparticle, then a large number of macrochain loops were formed, which were extended along the polarization axis of the nanoparticle. And when the distance between the oppositely charged units exceeded the diameter of the nanoparticle, then most of the charged units of the polypeptide were concentrated on the oppositely charged poles of the nanoparticle. In the case of MD simulation, on the surface of a germanium nanoparticle with a periodic change in its polarity in time at a small amplitude of the polarizing alternating electric field, an encircling annular polyampholytic fringe was formed in its equatorial region. With an increase in the amplitude of the polarizing alternating electric field, desorption of most of the polyampholyte units from the surface of the nanoparticle occurred.

Germanium nanoparticles with a macromolecular shell, the shape of which is sensitive to the action of an external electric field, can be used to create hybrid nanosystems with the possibility of field control of its plasmonic properties. Changes in the conformations of molecules of the surface layer of the polymer affect the effective value of the edge layer, and thus, the characteristics of the field outside the nanoparticle associated with its plasmonic properties. Such hybrid nanosystems with plasmon characteristics controlled by an electric field can find wide application in the creation of various chemical sensors, as well as nanoprobes in biomedicine.

REFERENCES

1 Lowe S.B., Dick J.A.G., Cohen B.E., et al. Multiplex sensing of protease and kinase enzyme activity via orthogonal coupling of quantum dot–peptide conjugates. *ACS Nano*, 2012, Vol. 6, pp. 851-857. doi:10.1021/nn204361s.

2 Yang L., Ahn D.J., Koo E. Ultrasensitive FRET-based DNA sensor using PNA/DNA hybridization. *Materials Science and Engineering: C*, 2016, Vol. 69, pp. 625-630. doi:10.1016/j.msec.2016.07.021.

3 Perng W., Palui G., Wang W., Mattoussi H. Elucidating the role of surface coating in the promotion or prevention of protein corona around quantum dots. *Bioconjugate Chem.*, 2019, Vol. 30. pp. 2469-2480. doi:10.1021/acs.bioconjchem.9b00549.

4 Green C.M., Spangler J., Susumu K., et al. Quantum dot-based molecular beacons for quantitative detection of nucleic acids with CRISPR/Cas(N) nucleases. *ACS Nano*, 2022, Vol. 16. pp. 20693-20704. doi:10.1021/acsnano.2c07749.

5 Jin Z., Dridi N., Palui G. et al. Quantum dot–peptide conjugates as energy transfer probes for sensing the proteolytic activity of matrix metalloproteinase-14. *Anal. Chem.*, 2023, Vol. 95, pp. 2713–2722. doi:10.1021/acs.analchem.2c034002713-2722.

6 Nejad Z.K., Khandar A.A., Khatamian M. Graphene quantum dots based MnFe2O4@SiO2 magnetic nanostructure as a pH-sensitive fluorescence resonance energy transfer (FRET) system to enhance the anticancer effect of the drug. *Intern. Journal of Pharmaceutics*, 2022, Vol. 628. pp. 122254. doi: 10.1016/j.ijpharm.2022.122254.

7 Tade R.S., Patil P.O. Fabrication of poly (aspartic) acid functionalized graphene quantum dots based FRET sensor for selective and sensitive detection of MAGE-A11 antigen. *Microchemical Journal*, 2022, Vol. 183, pp. 107971. doi:10.1016/j.microc.2022.107971.

8 Nevidimov. A.V., Razumov V.F. Nonradiative Energy Transfer in "Colloidal Quantum Dot Nanocluster–Dye" Hybrid Nanostructures: Computer Experiment. *High Energy Chemistry*, 2020, Vol. 54, pp. 28–35. https://doi.org/10.1134/S0018143920010105.

9 Nikolenko L.M., Pevtsov D.N., Brichkin S.B. Quantum-size effect for intraband electronic transition in colloidal silver selenide quantum dots. *High Energy Chemistry*, 2022, Vol. 56, pp. 380–382. doi:10.1134/S0018143922050125.

10 Cantini E., Wang X., Koelsch P., et al. Electrically Responsive Surfaces: Experimental and Theoretical Investigations. *Acc. Chem. Res.*, 2016, Vol. 49, pp. 1223–1231. doi:10.1021/acs.accounts.6b00132.

11 Zhao J., Wang X., Jiang N. et al. Polarization Effect and Electric Potential Changes in the Stimuli-Responsive Molecular Monolayers Under an External Electric Field. *J. Phys. Chem. C*, 2015, Vol. 119, pp. 22866–22881. doi:10.1021/acs.jpcc.5b04805.

12 Ghafari A.M., Domínguez S.E., Järvinen V. et al. In Situ Coupled Electrochemical-Goniometry as a Tool to Reveal Conformational Changes of Charged Peptides. *Advanced Materials Interfaces*, 2022, Vol. 9, pp. 2101480. doi:10.1002/admi.202101480.

13 Gomes B.S, Cantini E., Tommasone S. et al. On-Demand Electrical Switching of Antibody–Antigen Binding on Surfaces. *ACS Appl. Bio Mater.*, 2018, Vol. 1, pp. 738–747. doi:10.1021/acsabm.8b00201.

14 Kruchinin N.Y., Kucherenko M.G. Molecular-dynamics simulation of rearrangements in the conformational structure of polyampholytic macromolecules on the surface of a polarized metal nanoparticle. *Colloid Journal*, 2020, Vol. 82, pp. 136-143. doi:10.1134/S1061933X20020088.

15 Kruchinin N.Y., Kucherenko M.G. Conformational rearrangements of polyampholytic polypeptides on metal nanoparticle surface in microwave electric field: molecular-dynamics simulation. *Colloid Journal*, 2020, Vol. 82, pp. 392-402. doi:10.1134/S1061933X20040067.

16 Kruchinin N.Yu., Kucherenko M.G. Rearrangement of the conformational structure of polyampholytes on the surface of a metal nanowire in a transverse microwave electric field. *Eurasian phys. tech. j.* 2021, Vol.18, pp. 16-28. doi:10.31489/2021No1/16-28.

17 Kucherenko M.G., Kruchinin N.Yu., Neyasov P.P. Modeling of conformational changes of polyelectrolytes on the surface of a transversely polarized metal nanowire in an external electric field. *Eurasian phys. tech. j.* 2022, Vol. 19, pp. 19-29. doi:10.31489/2022No2/19-29.

18 Kruchinin N.Yu., Kucherenko M.G. Rearrangements in the conformational structure of polyampholytic polypeptides on the surface of a uniformly charged and polarized nanowire: Molecular dynamics simulation. *Surfaces and Interfaces*, 2021, Vol. 27, pp. 101517. doi:10.1016/j.surfin.2021.101517.

19 Kruchinin N.Yu., Kucherenko M.G. Molecular dynamics simulation of the conformational structure of uniform polypeptides on the surface of a polarized metal prolate nanospheroid with varying pH. *Russian Journal of Physical Chemistry A*, 2022, Vol. 96, pp. 624-632. doi:10.1134/S0036024422030141.

20 Kruchinin N.Yu., Kucherenko M.G. Modeling of electrical induced conformational changes of macromolecules on the surface of metallic nanospheroids. *Materials Today: Proceedings*, 2022, Vol. 71, Part 1, pp. 18-30. doi:10.1016/j.matpr.2022.07.139.

21 Kruchinin N.Yu., Kucherenko M.G. Rearrangements in the conformational structure of polyelectrolytes on the surface of a flattened metal nanospheroid in an alternating electric field. *Colloid Journal*, 2023, Vol. 85. pp. 44-58. doi:10.1134/S1061933X22600440.

22 Landau L.D., Pitaevskii L.P., Lifshitz E.M. Electrodynamics of Continuous Media, 2nd Edition, Elsevier Ltd., 1984, 460 p.

23 Grosberg A.Y., Khokhlov A.R. Statistical Physics of Macromolecules, 1994, AIP Press, New York. 347 p.

24 Klimov V.V. Nanoplasmonics, 2009, Moscow: Fizmatlit, 480 p. [in Russian]

25 Budak B.M., Samarskii A.A., Tikhonov A.N. Collection of problems in mathematical physics, 1979, M.: Science, 686 p. [in Russian]

26 Phillips J.C., Braun R., Wang W., et al. Scalable molecular dynamics with NAMD. *J Comput Chem.*, 2005, Vol. 26, pp. 1781-1802. https://doi.org/10.1002/jcc.20289.

27 MacKerell A.D. Jr., Bashford D., Bellott M., et al. All-atom empirical potential for molecular modeling and dynamics studies of proteins *J. Phys. Chem. B*, 1998, Vol. 102, pp. 3586-3616. doi:10.1021/jp973084f.

28 Huang J., Rauscher S., Nawrocki G. et al. CHARMM36m: an improved force field for folded and intrinsically dis-ordered proteins. *Nature Methods,* 2016, Vol.14, pp. 71-73. doi:10.1038/nmeth.4067.

29 Rappe A.K., Casewit C.J., Colwell K.S., et al. UFF, a full periodic table force field for molecular mechanics and molecular dynamics simulations. *J. Am. Chem. Soc.*, 1992, Vol. 114, pp. 10024–10035. doi:10.1021/ja00051a040.

30 Eidani M., Akbarzadeh H., Mehrjouei E., et al. Thermal stability and melting mechanism of diamond nanothreads: Insight from molecular dynamics simulation. *Colloids and Surfaces A: Physicochemical and Engineering Aspects*, 2022, Vol. 655, pp. 130248. doi:10.1016/j.colsurfa.2022.130248

31 Marashizadeh P., Abshirini M., Saha M., et al. Interfacial properties of ZnO nanowire-enhanced carbon fiber composites: a molecular dynamics simulation study. *Langmuir*, 2021, Vol. 37, pp. 7138–7146. doi:10.1021/acs.langmuir.1c00711.

32 Darden T., York D., Pedersen L. Particle mesh Ewald: An N·log(N) method for Ewald sums in large systems. *J. Chem. Phys.,* 1993, Vol. 98, pp. 10089-10092. doi:10.1063/1.464397.

33 Jorgensen W.L., Chandrasekhar J., Madura J.D., et al. Comparison of simple potential functions for simulating liquid water. *J. Chem. Phys.,* 1983, Vol. 79, pp. 926-935. doi:10.1063/1.445869.

34 Izmailov S.V. Electrodynamics course, 1962, M .: State educational and pedagogical publishing house of the Ministry of Education of the RSFSR, 439 p. [in Russian]

35 Shankla M., Aksimentiev A. Conformational transitions and stop-and-go nanopore transport of single-stranded DNA on charged grapheme. *Nat Commun.*, 2014, Vol. 5, pp. 5171. doi:10.1038/ncomms6171.